Supporting Information

Gallon et al. 10.1073/pnas.1410552111

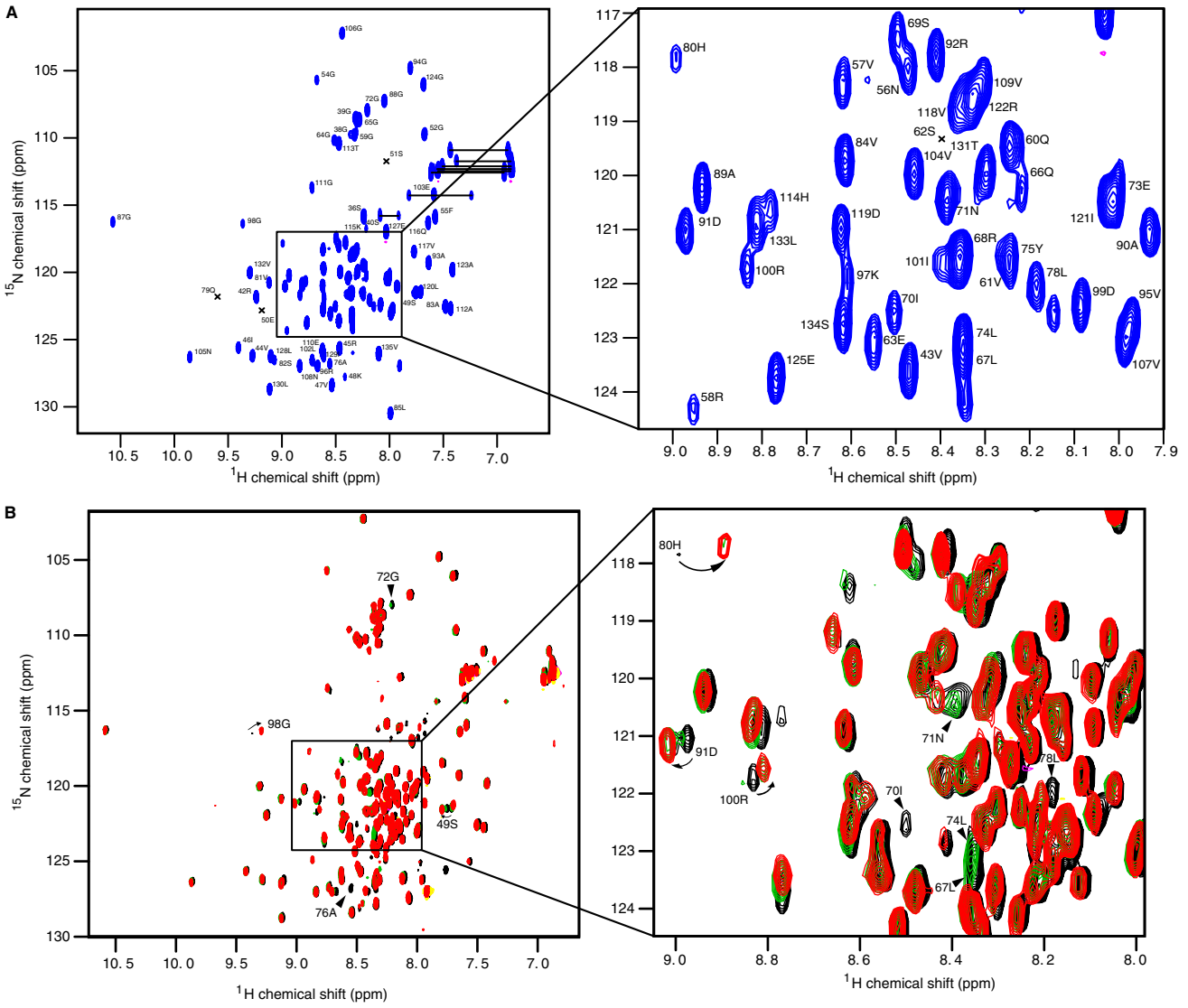

Fig. S1. Identification of the sorting nexin 27 (SNX27) binding surface on Vps26A using NMR (related to Fig. 1*C*). (*A*) 2D ^{1}H-^{15}N HSQC spectrum of Vps26A titration and resonance backbone assignment of SNX27PDZ. Data were recorded in 25 mM Hepes (pH 7.0) and 100 mM NaCl at 900 MHz and 25 °C. For the backbone assignment, horizontal lines connect peaks corresponding to NH_2 groups of asparagine and glutamine side chains. Signals too weak to be observed at this level are marked with a black cross and residue number. The region indicated by a rectangle is expanded for clarity. (*B*) Overlays of the 2D ^{1}H-^{15}N HSQC spectra of ^{15}N-^{13}C-labeled SNX27PDZ in its free form (black) and in the presence of 0.25 (green) and 2 (red) molar equivalents of unlabeled VPS26A. Resonances showing significant broadening and changes in chemical shift on VPS26A binding are labeled with the residue number.

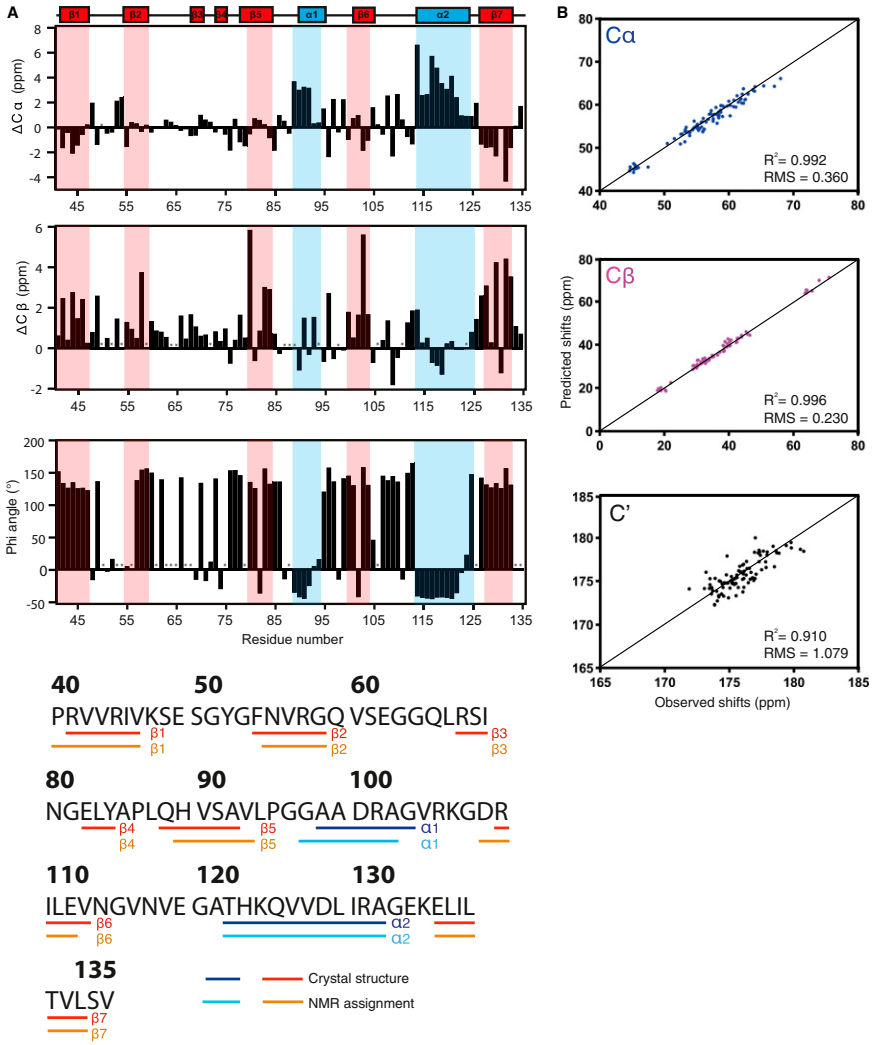

Fig. S2. The SNX27 protein in solution is the same as the crystalline form. (*A*) Cα and Cβ chemical shift deviations from random coil values along with the Phi angle values indicate a similar topology compared with the crystal structure. Secondary elements derived from the crystal structure are shown above, and predicted secondary structures from NMR analysis are shaded (β-sheets in red, α-helices in blue). (*B*) The Cα, Cβ, and C′ chemical shifts predicted by the ShiftX algorithm form the crystal structure correlate with those measured experimentally in this study. R^2 denotes the correlation coefficient, and rms values were calculated using $RMS = \sqrt{\sum (\sigma_{assigned} - \sigma_{predicted})^2}$.

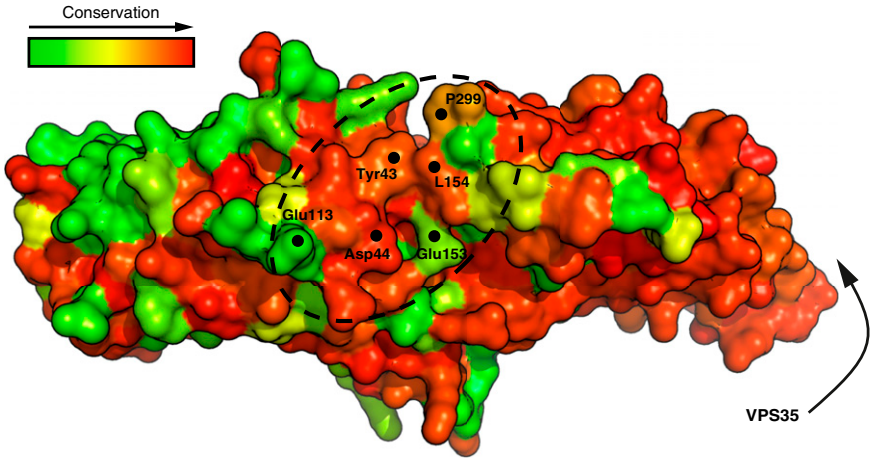

Fig. S3. SNX27PDZ L67 and L74 contact a hydrophobic cavity shaped by conserved residues on the VPS26A surface. Conserved residues in mammal VPS26A protein relatives were mapped onto the VPS26A surface (Fig. 2), colored from green to red, with increasing conservation score. A black dashed sphere indicates the SNX27PDZ interaction surface, and residues implicated in the interaction are depicted as dots. A black arrow indicates the conserved VPS35-binding surface on the C-terminal domain.

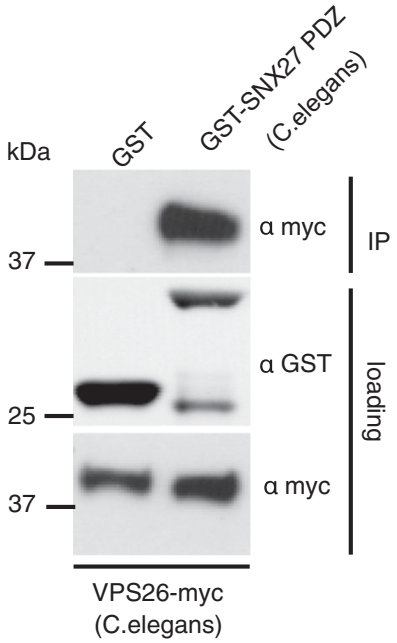

Fig. S4. Binding of SNX27 to VPS26 is conserved in *Caenorhabditis elegans*. The PDZ domain of *C. elegans* SNX27 fused to GST was purified from bacteria and tested for binding to purified *C. elegans* VPS26-myc in a direct binding assay.

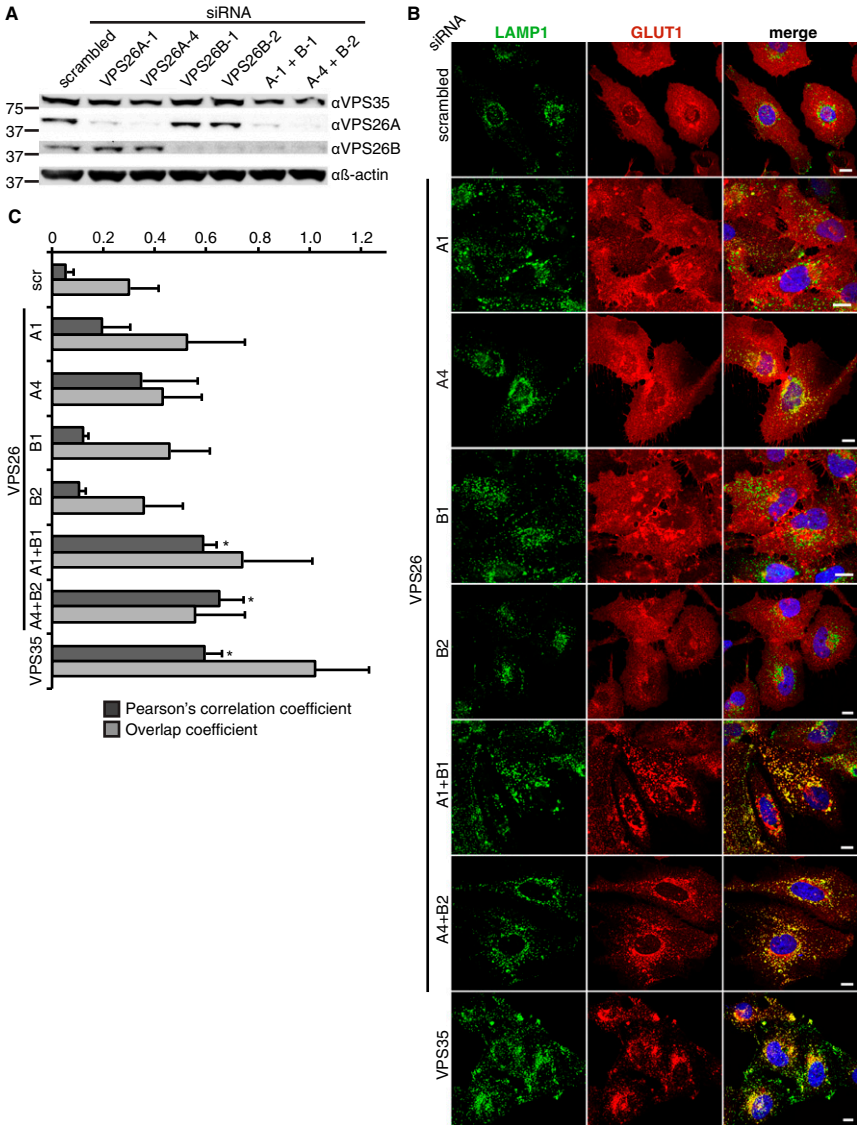

Fig. S5. VPS26 paralogues function redundantly in endosome-to-plasma membrane recycling of GLUT1. (*A*) VPS26A/B expression was suppressed in HeLa cells using each of four different oligonucleotides, then analyzed by resolving cell lysates using SDS/PAGE and probing with an antibody to VPS26A/B. (*B*) HeLa cells in which VPS26A and/or VPS26B expression had been suppressed using siRNA were stained for LAMP1 and GLUT1 and imaged on a confocal microscope. (Scale bar: 10 μm.) (*C*) Pearson's correlation coefficient (PCC) and overlap coefficient (Kx) for LAMP1 and GLUT1 in cells in which VPS26A and/or VPS26B expression was suppressed. The graph shows the mean of three independent experiments, in each of which at least 40 cells were analyzed. Error bars represent SD. *$P <$ 0.01, two-tailed *t* test compared with scrambled condition.

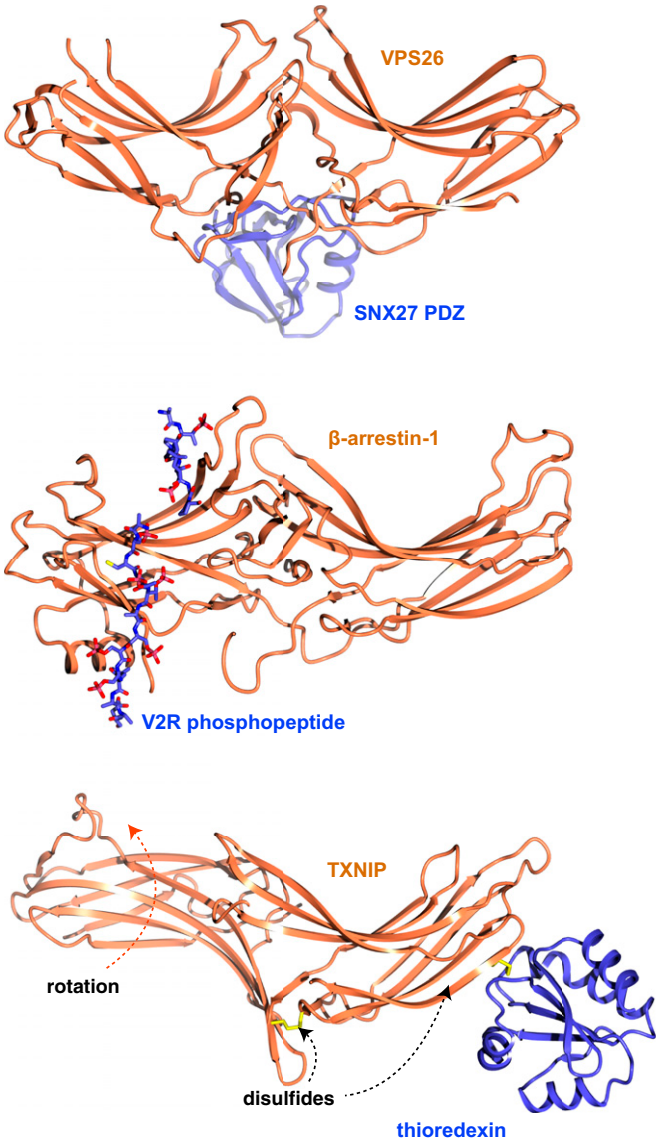

Fig. S6. Comparison of the VPS26-SNX27 complex to distantly related arrestin family members. The complex of VPS26 and the SNX27 PDZ domain is shown in a ribbon diagram (*Top*) and compared with the complex of β-arrestin1 bound to the phosphorylated peptide derived from the vasopressin 2 receptor (V2R) (Protein Data Bank ID code 4JQI) and the complex of TXNIP bound to thrioredoxin (*Middle*). Note that the thrioredoxin–TXNIP interaction involves disulphide bond exchange and a large rotational change in the relative orientations of the N- and C-terminal arrestin-fold subdomains compared with VPS26 and β-arrestins.

Table S1. Thermodynamic parameters for the binding of SNX27PDZ to peptides measured by isothermal titration calorimetry (related to Fig. 5*A*)

SNX27PDZ protein	Peptide*	K_d, μM	Δ*H*, kcal/mol	TΔ*S*, kcal/mol	Δ*G*, kcal/mol	N (stoichiometry)
WT	GLUT1	154 ± 11	ND[†]	ND	−5.2 ± 0.7	1[‡]
H114A	GLUT1	>200	ND	ND	ND	ND
WT + Vps26A	GLUT1	15 ± 0.8	−12.3 ± 0.3	−5.7 ± 0.3	−6.6 ± 0.4	1
WT + Vps26A L154A	GLUT1	90 ± 3.1	ND	ND	−5.5 ± 2.1	1
L74A + Vps26A	GLUT1	191 ± 33	ND	ND	−5.1 ± 1.9	1
WT	Kir3.3	17 ± 1.2	−21.4 ± 0.7	−14.9 ± 0.8	−6.5 ± 0.4	0.97 ± 0.03
H114A	Kir3.3	>200	ND	ND	ND	ND
WT + Vps26A	Kir3.3	1.1 ± 0.1	−23.1 ± 0.4	−15.0 ± 0.4	−8.1 ± 0.3	0.98 ± 0.03
WT + Vps26A L154A	Kir3.3	6.7 ± 0.3	−25.1 ± 0.3	−18.0 ± 0.3	−7.1 ± 0.1	0.95 ± 0.01

All isothermal titration calorimetry measurements are given as average ± SD from three independent experiments.
*Synthetic 8-aa peptides used in this study were GLUT1 (PLGADSQV) and Kir3.3 (PPESESKV).
[†]ND, not determined. For low affinity interactions with GLUT1 peptides, calculation of Δ*H* (and TΔ*S*) was unreliable.
[‡]Stoichiometry was manually fixed to 1.0 to improve the curve fitting.